Journal of Applied Fluid Mechanics, Vol. 10, No. 4, pp. 1125-1138, 2017.
Available online at www.jafmonline.net, ISSN 1735-3572, EISSN 1735-3645.
DOI: 10.18869/acadpub.jafm.73.241.26514

Effect of Rayleigh Number with Rotation on Natural Convection in Differentially Heated Rotating Enclosure

M. Narendra Kumar[1], G. Pundarika[2], K. R. Narasimha[3] and K. N. Seetharamu[4]

[1] *Centre for Incubation, Innovation, Research and Consultancy (CIIRC), Jyothy Institute of Technology, Bengaluru, Karnataka, 560082, India*
[2] *Government Engineering College, Ramanagara, Karnataka, 571511, India*
[3] *KS Institute of Technology, Bengaluru, Karnataka, 560062, India*
[4] *PES University, Bengaluru, Karnataka, 560085, India*

†*Corresponding Author Email:naru_sa@yahoo.co.in*

(Received May 7, 2016; accepted March 15, 2017)

ABSTRACT

A Numerical study is carried out to investigate the effect of Rayleigh number with rotation on the flow and heat transfer characteristics in a differentially heated enclosure rotating about the horizontal axis. A Fortran Code developed based on FVM is used to discretize governing equations. Upwind difference scheme for convective terms and fully implicit scheme for transient terms are used. The SIMPLE algorithm is employed to couple pressure and velocities on staggered grid arrangement. The results were obtained for a Taylor number($10^3 \leq Ta \leq 10^5$), rotation ($10\ rpm \leq \Omega \leq 25\ rpm$), and Rotational Rayleigh number ($10^1 \leq Ra_w \leq 10^3$) for two different Rayleigh number (1.3×10^4 & 1.1×10^5) with fixed Prandtl number ($Pr = 0.71$). The results showed that the Coriolis force first tends to decrease heat transfer to a minimum and then starts to increase it with increase Rayleigh number and rotation. Minimum depends on Rayleigh number and corresponds to the balanced effects of interacting forces at the point of transition. At rotations, below minimum in average heat transfer, the circulations are counter clockwise. The direction of coriolis force is from core region, so both flow and heat transfer is reduced. When coriolis force is much larger than thermal buoyancy, motion is clockwise, and transition is prevented. coriolis force now tends to promote flow circulation and therefore increases the heat transfer. The frequency content of flow pattern reveals the structural changes in the flow and temperature fields with increasing Rayleigh number and rotation. The existence of different flow regimes dominated by these body forces complicates the time average heat transfer characteristics with a different behaviour in each of the regimes.

Key words: Rayleigh number; Taylor number; Rotating enclosure; Natural convection; Coriolis force.

NOMENCLATURE

CEF	Dimensionless Centrifugal Force	T_h	temperature of hot wall
COF	Dimensionless Coriolis Force	T_c	temperature of cold wall
$\vec{g}$	gravity vector	T	temperature
k	thermal conductivity	TBF	dimensionlessThermal Buoyancy
L	length of enclosure	Ta	Taylor Number
Nu	local Nusselt number	U, V	dimensionless velocity component
$\overline{Nu}$	space average Nusselt number	u, v	dimensional velocity components
$\overline{\overline{Nu}}$	time average Nusselt number	V_R	dimensionless resultant velocity
n	revolutions	V	velocity vector
P	dimensionaless pressure	X, Y	dimensionaless cartesion coordinates
Pr	Prandtl Number	x, y	dimensional cartesion coordinates
P_m	motion pressure		
Ra_ω	Rotational Rayleigh Number	α	thermal diffusity
Ra	Rayleigh Number	β	voefficient of thermal expansion
t	time	θ	dimensionless temperature
T_0	intial temperature	μ	dynamic viscosity

ρ	density	Ω	rotation
τ	dimensionless time	ω	angular velocity
ϕ	angular position of enclosure	f	dimensionless frequency

1. INTRODUCTION

Natural convection in rotating enclosure is very different from stationary enclosure. When the enclosure is rotated, the flow in it is simultaneously affected by the coriolis and centrifugal forces as well as the thermal buoyancy. Natural convection flows in rotating enclosure are important in many engineering applications such as nuclear power plants, cooling of electronic systems, atmospheric re-entry of space vehicles, gas turbines, spin-stabilized missiles, and cooling of conventional rotating machinery such as electrical motors, turbines, guided missiles, manufacturing of single crystal wafer and space-based manufacturing processes etc. Natural convection in a rotating system also finds applications in petroleum engineering for observing the movement of oil and gas through a reservoir. When natural convection takes place in a rotating enclosure, transport processes, involving the coupling of fluid flow and heat transfer, become more challenging in view of the complexities arising out of rotation and increased number of parameters emanating from pseudo forces. These forces arising due to rotation makes the flow and heat transfer characteristics more complex and still need to be explored.

Most of the early studies initially focused only on the heat transfer in rotating cylindrical enclosure. Both theoretical and experimental studies, exists in the open literature related to flow and heat transfer in circular cylinder. Ostrach (1950) considered the steady laminar flow generated in a horizontal cylinder by an imposed cosine temperature distribution on the cylinder wall. The temperature extremes were along the horizontal diameter. Weinbaum (1964) investigated the convection phenomenon in a horizontal cylinder for different locations of temperature extremes on wall of the cylinder. He also carried out a linear stability analysis for the bottom heating case. Brooks and Ostrach (1970) experimentally investigated natural convection in a horizontal cylinder by varying the location of the temperature extremes on the periphery of the cylinder. Numerical study by Veronis (1968) revealed the significant effects of Prandtl number on the flow and thermal structures. For the limit of an infinite Prandtl number Kupper and Lortz (1969) showed that no stable steady state convective flow exists beyond a certain critical value of Taylor number. Rossby (1969) experimentally observed the subcritical instability in a water layer for $Ta > 10^5$ and in an air layer for $Ta < 10^5$. In addition, for water at $Ra > 10^4$, the Nusselt number was found to increase with the Taylor number. The opposite trend is observed for air. Besides, at a large Taylor number oscillatory convection is preferred in mercury. Mori *et al.* (1971) studied the laminar as well as turbulent heat convection with fully developed velocity and temperature fields in a circular pipe rotating around an axis perpendicular to its own axis. Their analysis revealed that the flow resistance coefficient and Nusselt number (Nu) increased remarkably due to a secondary flow driven by the Coriolis force for laminar case; whereas the influence of the secondary flow and increase in Nu is less in case of turbulent flow as compared to laminar flow. Thermal convection in a vertical rotating cylinder heated from above has been studied by Homsy and Hudson (1971) and Abell and Hudsen (1975). Difference between rotating and non rotating convection were presented in terms of the centrifugal acceleration, which is a strong function of the radial position, and the Coriolis acceleration, which contributes significantly to the heat transfer as a consequence of the induced secondary flow. Pfotenhauer *et al*. (1987) reported experimental results for the effects of the cylinder geometry and rotation on the onset of convection for low temperature liquid helium. Both the Rayleigh number associated with the convective onset and the convection heat transfer were found to depend on the rotation rate and aspect ratio of the cell. Numerical investigation of Xin *et al*. (1997) have provided detailed information regarding flow structure and heat transfer for a range of Rayleigh and Prandtl numbers for the case of temperature extremes along the horizontal diameter. Their investigation revealed that the flow is essentially of the boundary layer type with motion confined to a thin layer close to the cylinder wall and the core being nearly isothermal and stagnant. They also carried out a linear stability analysis to determine the critical Rayleigh number for the loss of stability of steady convection. Ker *et al*. (1998) experimentally studied the flow stabilization by rotation in convection of air in a vertical circular cylinder heated from below. Their investigation relived that for a given ΔT two different ranges of rotation exist for the flow to be stabilised. Outside these ranges the flow oscillates periodically or quasi-periodically in time. At given ΔT and rotation, the temperature oscillation at various locations exhibits some change in amplitude with negligible change in frequency. However, change of the oscillation frequency with rotation is non-monotonic and is rather significant at high rotation rates. But this frequency changes when the imposed ΔT is small. Yin *et al*. (2001) carried out experimental studies to investigate the fluctuating characteristics and stabilization of the thermal buoyancy driven water flow in a vertical axis rotating cylinder heated from below. They found that the flow suppression by cylinder rotation causes the time average temperature distribution along the cylinder axis for high rotation to become linear. Besides, a finite range of the rotation exits for the thermal buoyancy driven flow to be stabilized. Significant dependence of the oscillations amplitude was revealed. Moreover, a non-monotonic variation of the oscillation frequency with rotation rate was observed. Hasan and Sanghi. (2004, 2007)

conducted a study on a 2D thermally driven flow of air in a steadily rotating horizontal cylinder. In their numerical investigation, a spatially periodic temperature variation is imposed on the circular wall of the cylinder. The investigation was carried out in a Cartesian rotating frame of reference. The changes in the spatial and temporal structure of the unsteady flow at a fixed Rayleigh number and Prandtl number as Rotational Rayleigh number was varied from 10^2 to 10^7 were studied.

Many researches are also carried out to study the effects of the rotation in non circular rotating enclosure due to its significance in varied application. Hamady *et al*. (1994) investigated, both experimentally and numerically two dimensional natural convection in an air filled differentially heated square enclosure rotating about an axis perpendicular to the plane of motion. Their investigation was carried out at low enough rotation rates so that the centrifugal or rotational buoyancy was insignificant. They concluded that the Coriolis force arising from rotation may have a remarkable influence on heat transfer when compared to non rotating results. Lee and Lin (1996, 1997) numerically investigated the three dimensional flow in a rotating, differentially heated cubical enclosure rotated about vertical axis. Significant flow modifications are obtained when the rotational Rayleigh number is greater than the conventional Rayleigh number. Ker and Lin (1997) experimentally and numerically investigated three dimensional flows in a tilted, rotating differentially heated cubical cavity for the case of the rotation axis perpendicular to the component of gravity. They found that the oscillation levels of the flow field and the heat transfer rates could be effectively controlled using rotation. However, their carried out study have not correlated the flow structure to the different body forces involved. Further, they have not investigated the effects of rotation of the gravity vector on the flow structure. The study of Baig and Masood (2001) involved a numerical investigation of the two dimensional convection of air in a rotating square enclosure. Some of the features of the flow observed in the numerical experiments were attributed to the coriolis force. In particular it was concluded that the effect of the coriolis force is to create convective motion in the core of the cavity. It was also reasoned that the stratification in the core becomes unstable and reversal of the flow in the core was observed whenever Coriolis forces dominated the flow. Baig and Zunaid (2006) carried out numerical investigation to examine the characteristics of mixed convective heat transfer in square enclosures undergoing rotation about horizontal axis. Results revealed significant increase or decrease in heat transfer rates could be achieved by rotational effects, mainly influenced by centrifugal force. Jin *et al*. (2005) studied numerically a rectangular enclosure with discrete heat source and found that rotation results in imbalance of clockwise circulations. Tso *et al*. (2007) carried out numerical studies to investigate the effects of Coriolis force, centrifugal force and thermal buoyancy force in a rotating differentially heated square enclosure. Their studies focused on the evaluation of the flow pattern in the natural convection flow fields for different rotation rates of the enclosure. They found the effects of Coriolis force and centrifugal force are small and are differentiated from those of other forces. Mandal *et al*. (2013) carried out numerical studies on orthogonal rotating square cavity using Non Inertial (NI) frame of reference with explicit treatment of source term, NI frame of reference with implicit treatment of source term and then using inertial frame of reference and found that the results of both the formulations match well for low rotational speeds of the cavity. The discrepancies between the results of the two formulations progressively increase with the increase in rotational speed. Implicit treatment of the source term is found to reduce the discrepancies. Narendra kumar *et al.* (2016) carried out numerical studies to investigate the effects of pseudo forces and thermal buoyancy force in a rotating differentially heated square enclosure. Their studies focused on the evaluation of the flow pattern in the natural convection flow fields for different rotation of the enclosure. Masuda *et al.* (2010) numerically investigated the ammonothermal process for growing GaN bulk single crystals for flat and funnel shaped baffles The results obtained were identical to that on the hydrothermal ZnO crystal growth process. Masuda *et al.* (2016) numerically studied the natural convection heat transfer in an ammonothermal process for growing GaN bulk single crystals. They considered only one crystal to simplify the calculation and discuss the relationship between convection patterns and temperature fields. Two types of convection patterns were observed owing to the difference in the crystal radius. When the convection pattern is transformed, the crystal surface temperature decreases with increase in crystal radius.

From the literature review, it is observed that a significant amount of research has been done on rotating enclosure with vertical axis of rotation aligned parallel to the gravity vector. Invariably in all these studies, either neglecting Centrifugal buoyancy forces so that the results apply only for low rotation rates governed by the condition centrifugal acceleration or gravitational acceleration $<<1$ and vice versa. In these numerical works, both rigid as well as stress free boundaries were treated. However, the configurations having either the gravity or its component perpendicular to the axis of rotation have been far less explored. The thermally driven flow in such configurations is driven by an unsteady gravitational buoyancy force as a result of changing orientation of the gravity vector with respect to the frame attached with the rotating enclosures. However Studies by Ker *et al*. (Ker and Lin, 1996), Hamady *et al*. (1994), Baig *et al*. (2001, 2006), Mandal *et al*. (2013) and Narendra kumar *et al.* (2016) are a few isolated works on configurations involving a time-periodic gravitational buoyancy force. The influence of Coriolis force in low rotation speed range on the thermal buoyancy with horizontal axis of rotation of enclosure is far less explored in the open literature, The literature review indicates that the previous studies mainly focused on the effects of the rotation on the onset of convection and overall heat transfer at given Rayleigh numbers. Most

reported work on natural convection rotating enclosure has the gravitational force parallel to the rotating axis, but if the gravitational force is not parallel to the rotating axis, the flow and heat transfer field may undergo a fundamental change when the buoyancy force is considered. Despite it being fundamentally important in understanding the complex coupling among the various body forces, numerical studies in this field are limited. The purpose of the present work is to study the effects of Rayleigh number with rotation on pseudo forces produced by rotation namely the Coriolis and centrifugal forces and to determine how these pseudo forces interact with the thermal buoyancy, influencing the flow and heat transfer characteristics in the differentially heated rotating enclosure.

2. MATHEMATICAL MODEL

The schematic representation of the physical system under investigation is shown in Fig. 1. A square geometry which contains air as the working fluid is considered. Initially at time $t = 0$, the enclosure is rotated at a constant angular speed Ω about an axis through the centre of the enclosure and is isothermal at temperature T_o. At time $t > 0$, the wall temperatures of the enclosure are suddenly raised and lowered to some uniform constant temperature conditions in the following manner. The surface at $Y = L/2$ is subjected to uniform temperature T_h and the surface at $Y = -L/2$, subjected to uniform temperature T_c. The lateral walls are thermally well insulated from the surroundings.

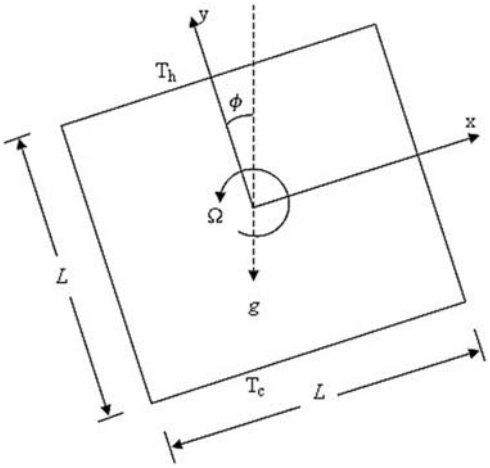

Fig. 1. Schematic representation of the physical system.

The ϕ in Fig. 1 defines the angular position of the enclosure. Thus the air flow inside the enclosure is simultaneously driven by the rotation and the thermal buoyancy. By using the Boussinesq approximation, [Buhler *et al*., (1982). Lee *et al*., (1996) and Jin *et al*., (2005)] in which linear density variation with temperature is considered in both the body force and centrifugal force terms, the terms representing the thermal and rotational buoyancies and Coriolis force are, respectively, equal to $\rho_o \vec{g}\beta(T - T_c)$, $-\rho_o\beta(T - T_c)\vec{\Omega} \times (\vec{\Omega} \times \vec{r})$ and $-2\rho_o\,[1 - \beta(T - T_c)]\Omega \times \mathrm{V}$. The resulting flow development can be described as follows:

The continuity, momentum and energy equations are

$$\frac{\partial u}{\partial x} + \frac{\partial v}{\partial y} = 0 \tag{1}$$

$$\frac{\partial u}{\partial t} + u\frac{\partial u}{\partial x} + v\frac{\partial u}{\partial y} = -\frac{1}{\rho_o}\frac{\partial P_m}{\partial x} + \nu\left(\frac{\partial^2 u}{\partial x^2} + \frac{\partial^2 u}{\partial y^2}\right) + g\beta(T - T_C)sin(\Omega t)$$

$$-\Omega^2 x\beta(T - T_C) + 2\Omega v \tag{2}$$

$$\frac{\partial v}{\partial t} + u\frac{\partial v}{\partial x} + v\frac{\partial v}{\partial y} = -\frac{1}{\rho_o}\frac{\partial P_m}{\partial y} + \nu\left(\frac{\partial^2 v}{\partial x^2} + \frac{\partial^2 v}{\partial y^2}\right) + g\beta(T - T_C)cos(\Omega t)$$

$$-\beta\Omega^2 y(T - T_C) - 2\Omega u \tag{3}$$

$$\frac{\partial T}{\partial t} + u\frac{\partial T}{\partial x} + v\frac{\partial T}{\partial y} = \alpha\left(\frac{\partial^2 T}{\partial x^2} + \frac{\partial^2 T}{\partial y^2}\right) \tag{4}$$

The Boundary Conditions are

$$\left\{\begin{array}{ll} at\ x = -\,{}^{L}/_{2}, u = v = 0, & \dfrac{\partial T}{\partial y} = 0 \\ at\ x = {}^{L}/_{2}, u = v = 0, & \dfrac{\partial T}{\partial y} = 0 \\ at\ y = -\,{}^{L}/_{2}, u = v = 0, & T = T_C \\ at\ y = {}^{L}/_{2}, u = v = 0, & T = T_h \end{array}\right\} \tag{5}$$

With the motion pressure defined as

$$P_m = p - \frac{1}{2}\rho_o\Omega^2 x^2 - \frac{1}{2}\rho_o\Omega^2 y^2 + \rho_o gxsin(\Omega t) + \rho_o gycos(\Omega t) \tag{6}$$

Hence,

$$-\frac{\partial P_m}{\partial x} = -\frac{\partial p}{\partial x} + \rho_o\Omega^2 x - \rho_o gsin(\Omega t) \tag{7}$$

$$-\frac{\partial P_m}{\partial y} = -\frac{\partial p}{\partial y} + \rho_o\Omega^2 y - \rho_o gcos(\Omega t) \tag{8}$$

As mentioned by Vanyo (1993) in a rotating reference frame, the centrifugal term can be included in the pressure term and disappears from the typical rotating fluid computation. With Boussinesq approximation, the main part of the centrifugal force term is combined with the pressure term and others are caused by density change and centrifugal buoyancy. The governing equations can be converted to non-dimensional forms using the non-dimensional parameters as indicated in (9).

$$\left\{\begin{array}{l} X = \dfrac{x}{L}\ \ Y = \dfrac{y}{L}\ \ U = \dfrac{uL}{\alpha}\ \ V = \dfrac{vL}{\alpha}\ \ \tau = \dfrac{t\alpha}{L^2} \\ P = \dfrac{P_m L^2}{\rho\alpha^2}\ \ \theta = \left(\dfrac{T - T_C}{T_h - T_C}\right)\ Ra = \dfrac{g\beta(T_h - T_C)L^3}{\nu\alpha} \\ Pr = \dfrac{\nu}{\alpha}\ \ Ra_w = \dfrac{\beta\Omega^2(T_h - T_C)L^4}{\nu\alpha}\ \ Ta = \dfrac{4\Omega^2 L^4}{\nu^2} \end{array}\right\} \tag{9}$$

The dimensionless governing equations and the

relevant boundary conditions are written as follows

Continuity equation:

$$\frac{\partial U}{\partial X}+\frac{\partial V}{\partial Y} \quad = 0 \tag{10}$$

Momentum equations:

$$\frac{\partial U}{\partial \tau}+U\frac{\partial U}{\partial X}+V\frac{\partial U}{\partial Y}=-\frac{\partial P}{\partial X}+Pr\left(\frac{\partial^2 U}{\partial X^2}+\frac{\partial^2 U}{\partial Y^2}\right)+(Ta^{0.5}PrV)$$

$$-(Ra_w Pr\theta X)+(RaPr\theta \sin(0.5Ta^{0.5}Pr\tau) \tag{11}$$

$$\frac{\partial V}{\partial \tau}+V\frac{\partial V}{\partial X}+V\frac{\partial V}{\partial Y}=-\frac{\partial P}{\partial Y}+Pr\left(\frac{\partial^2 V}{\partial X^2}+\frac{\partial^2 V}{\partial Y^2}\right)-(Ta^{0.5}PrU)-(Ra_w Pr\theta Y)+(RaPr\theta\cos(0.5Ta^{0.5}Pr\tau) \tag{12}$$

Energy equation:

$$\frac{\partial \theta}{\partial \tau}+U\frac{\partial \theta}{\partial X}+V\frac{\partial \theta}{\partial Y}=\frac{\partial^2 \theta}{\partial X^2}+\frac{\partial^2 \theta}{\partial Y^2} \tag{13}$$

Boundary Conditions:

$$\left.\begin{array}{llll} at\ X=-0.5, & U=V=0, & \dfrac{\partial\theta}{\partial Y}=0 \\ at\ X=\ 0.5, & U=V=0, & \dfrac{\partial\theta}{\partial Y}=0 \\ at\ Y=-0.5, & U=V=0, & \theta=-0.5 \\ at\ y=\ 0.5, & U=V=0, & \theta=0.5 \end{array}\right\} \tag{14}$$

In the present case, the fluid is an air with low viscosity under laminar flow situations. Therefore, the change in internal energy due to viscous dissipation will not influence the internal energy significantly and, subsequently, the temperature. As a result, it can be neglected in equation (4) and (13). Moreover, viscous dissipation becomes important when the fluid is highly viscous or turbulent. The above formulation clearly shows that the flow to be examined is governed by dimensionless parameters, namely Prandtl number, Rayleigh number, Taylor number and rotational Rayleigh number. The rotational Rayleigh number which reflects the effect of the rotational buoyancy force depends on the other non-dimensional parameters. The rotational buoyancy becomes important when the rotational speed is high or the enclosure dimensions are too large, viz when Ω^2L is much larger than g [Lin *et al*. (1996)].

The fluid motion is displayed using the stream function obtained from the velocity components *U* and *V* and the temperature fields using the isotherms. In addition to the time evaluation of velocity and temperature fields, results for the local, space averaged and time space averaged Nusselt number (*Nu*) on the heated or cooled wall are important in thermal design and can be evaluated from

$$\left.\begin{array}{l} Nu=\left.\dfrac{\partial\theta}{\partial Y}\right|_{Y=\pm 0.5} \\ \overline{Nu}=\displaystyle\int_{-0.5}^{0.5} NudX \\ \overline{\overline{Nu}}=\dfrac{1}{2\pi}\displaystyle\int_0^{2\pi}\overline{Nu}d\phi \end{array}\right\} \tag{15}$$

3. NUMERICAL APPROACH

An in-house Fortran Code is developed using finite volume methodology to solve equation (10) – (13). Furthermore, equations (10) – (13) are written in a general form as given by equation (16) and then Patakar's SIMPLE algorithm is applied

$$\frac{\partial \rho\varphi}{\partial t}+div(\rho\varphi U)=div(\Gamma grad\varphi)+S_\varphi \tag{16}$$

Where, φ is a conservative form of all fluid flow, ρ is density, $div(\rho\varphi U)$ is a net rate of flow of φ out of the fluid element represents convective term, $div(\Gamma grad\varphi)$ is a rate of change φ of due to diffusion, S_φ is a rate of increase of φ due to source and $\frac{\partial\rho\varphi}{\partial t}$ is a transient term.

The terms φ, Γ_φ and S_φ are determined and then the equations are solved simultaneously. The upwind differencing scheme for treating convective terms and the fully implicit procedure to discretize the temporal derivatives are retained. The SIMPLE algorithm is utilised to couple the pressure and velocities on staggered grid arrangement. The resulting discretized equations are solved by a line by line solution method in conjunction with the tri-diagonal matrix algorithm (TDMA), enforcing under-relaxation to ensure convergence at each time step. In the iteration procedure, the motion pressure correction equations are used to derive the new velocity from the previous calculated velocity. To check the convergence, the maximum residual of mass, momentum and energy all nodes of computation domain are selected to be 0.00001 to ensure convergence at each time step level.

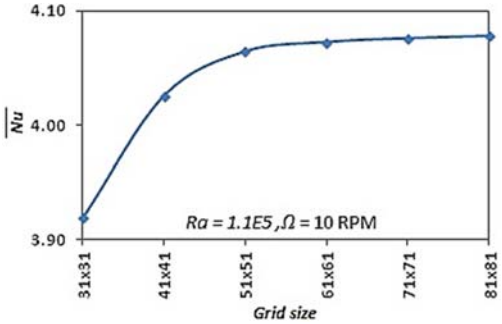

Fig. 2. Grid independency study of space average Nusslet number with grid size.

4. GRID INDEPENDENCE STUDIES

In order to determine the proper grid size for the study, a grid independency study is performed using six different uniform staggered grids of 31×31,

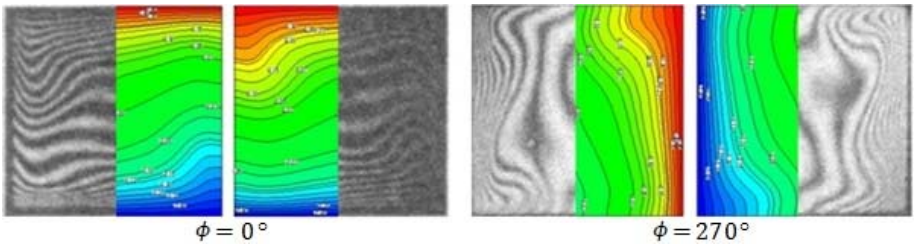

Fig. 3. Comprasion of Isotherms of the present work with experimental result of Hamady *et al*.

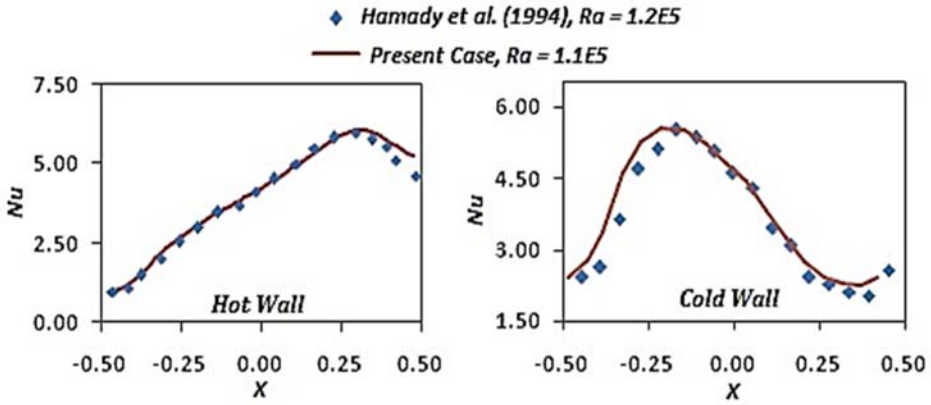

Fig. 4. Comparison of the local Nusselt number for $\phi = 270^0$, $\Omega = 15\ rpm$ with experimental result of Hamady *et al*.

41×41, $51 \times 51, 61 \times 61, 71 \times 71$ and 81×81. The space average Nusselt number is used as a parameter to check the grid independency of the results, which is shown in Fig. 2. For $Ra = 1.1 \times 10^5$ & $\Omega = 10\ rpm$. The comparison of the five grid results indicates the grid independency of the numerical code implemented here. Considering both the accuracy of numerical value and computational time, the present calculations are performed with 61×61 grids.

5. CODE VALIDATION

In view of the complex flow to be simulated, program tests are conducted to verify the proposed solution method for rotating enclosure. The present results were compared with the experimental data of Hamady *et al*. (1994) for a typical case $Ra = 1.1 \times 10^5$ and $\Omega = 15\ rpm$. The present results of the code for isotherms compare well with the experimental result obtained by Hamady *et al*. (1994) for two angular postion of the enclosure as shown in Fig. 3. The present results for local Nusselt number at hot and cold wall for $\phi = 270^o$ position of the enclosure are in good agreement with the results of experimental data of Hamady *et al*. (1994) as depicted in Fig. 4. Furthermore, results for the transient variation of the space averaged Nusselt number on the hot wall at $\phi = 270^o$ position of the enclosure for various Ta for fixed Ra are also in good agreement with experimental data of Hamady *et al*. (1994) as depicted in Fig. 5. Good agreement is noted for the entire transient case.

6. RESULTS

In the present work, the natural convection in the differentially heated rotating enclosure is studied for a range of Taylor number ($10^3 \leq Ta \leq 10^5$), rotation rates ($10\ rpm \leq \Omega \leq 25\ rpm$) and Rotational Rayleigh number ($10^1 \leq Ra_w \leq 10^3$) for two different Rayleigh number ($Ra = 1.3 \times 10^4$ & 1.1×10^5) and for a fixed Prandtl number $Pr = 0.71$ with air as the working medium in the rotating enclosure. The Rotational Rayleigh number is not discussed except to specify it explicitly. The results of the simulations are divided into six sections.

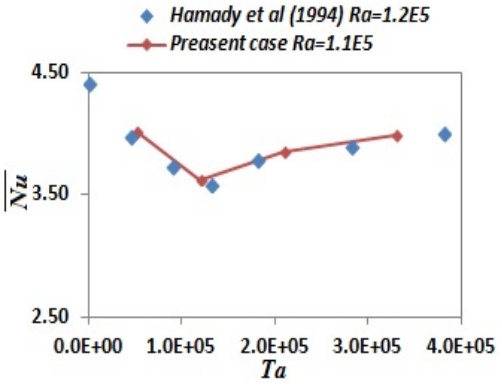

Fig. 5. Comparison of the space average Nusselt number for $\phi = 270^0$ with experimental result of Hamady *et al*.

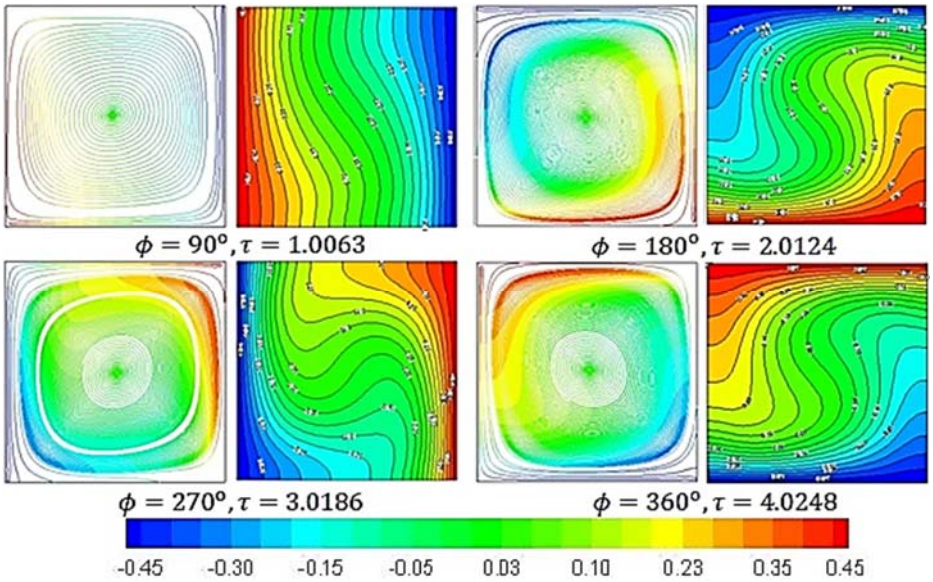

Fig. 6. Instantaneous Flow and Temperature field in rotating enclosure $(\boldsymbol{Ra = 1.3 \times 10^4}$ & $\boldsymbol{\Omega = 10\ rpm})$.

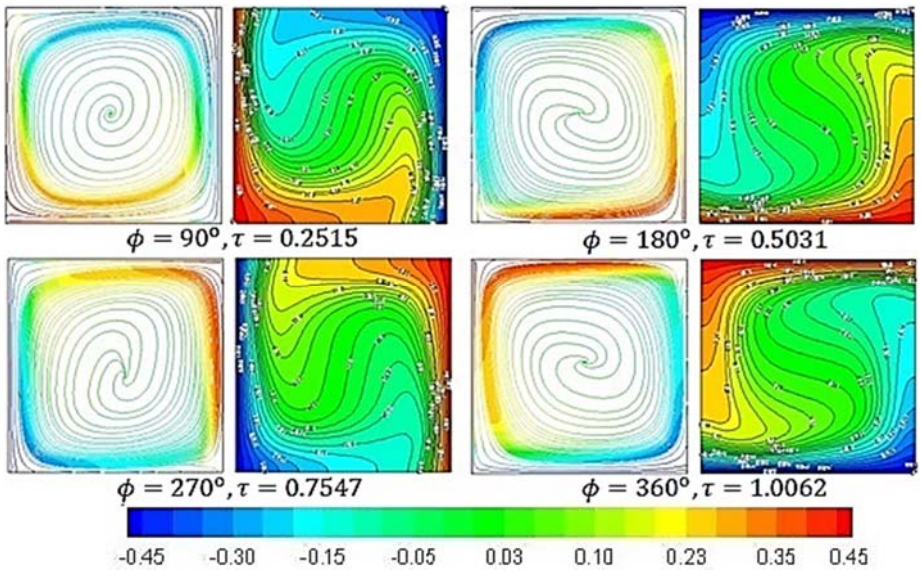

Fig. 7. Instantaneous Flow and Temperature field in rotating enclosure $(\boldsymbol{Ra = 1.1 \times 10^5}$ & $\boldsymbol{\Omega = 10\ rpm})$.

6.1 Effect of Rayleigh Number with Rotation on Flow and Temperature Tields

Figure 6 to 9 represents the instantaneous streamline and isotherm at different angular position of the enclosure. At $\phi = 90^o$ angular position, the hot isothermal wall occupies the left vertical position. At $\phi = 180^o$ angular position, the hot isothermal wall occupies the bottom horizontal position. At $\phi = 270^o$ angular position, the hot isothermal wall occupies the right vertical position and at $\phi = 360^o$ angular position, the hot isothermal wall occupies the top horizontal position.

For $\Omega = 10\ rpm$ at $Ra = 1.3 \times 10^4$, The flow is driven by thermal buoyancy with counter clockwise flow circulations compared to smaller magnitude of coriolis forces as shown in Fig. 6, which shows unicellular roll pattern of streamlines. The isotherm departs from the vertical position. As time progresses, the heat transfer changes from conduction to convection with thin boundary layer near isothermal walls with stable stratification of the core as seen in Fig. 6. With increase in Ra to 1.1×10^5, the flow is still dominated by thermal buoyancy with counter clockwise flow circulations compared to smaller magnitude of coriolis forces. The streamlines shows unicellular roll pattern of slightly larger magnitude as shown in Fig. 7. The isotherm demonstrates thin boundary layer near the isothermal

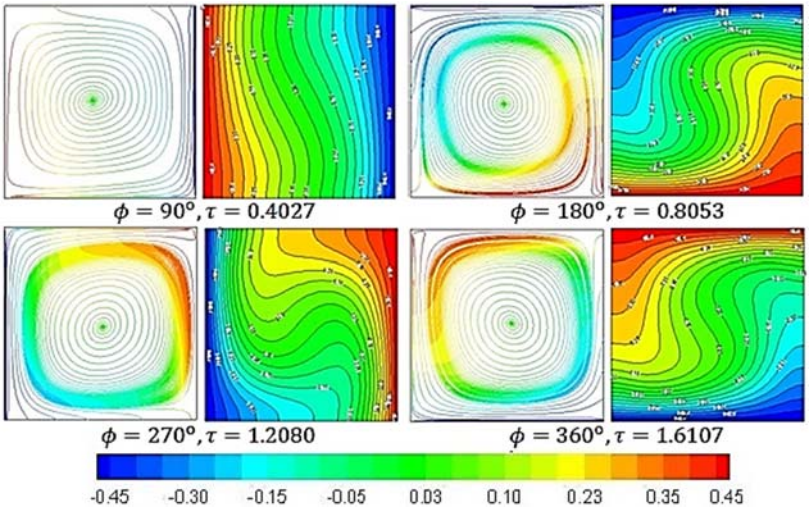

Fig. 8. Instantaneous Flow and Temperature field in rotating enclosure $(\boldsymbol{Ra = 1.3 \times 10^4}$ & $\boldsymbol{\Omega = 25\ rpm})$.

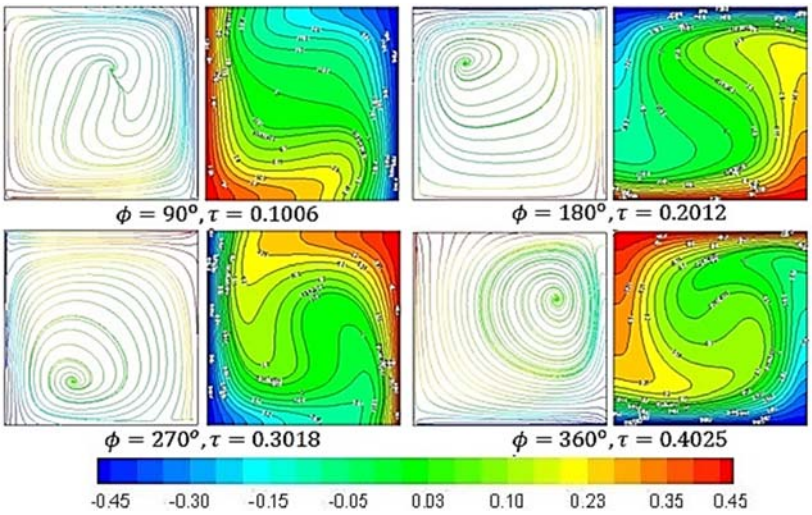

Fig. 9. Instantaneous Flow and Temperature field in rotating enclosure $(\boldsymbol{Ra = 1.1 \times 10^5}$ & $\boldsymbol{\Omega = 25\ rpm})$.

wall with stable stratification of the core as shown in Fig. 7. For $\Omega = 25\ rpm$ at $Ra = 1.3 \times 10^4$, The flow is still driven by thermal buoyancy with counter clockwise flow circulations compared to smaller magnitude of coriolis forces as shown in Fig. 8 which shows unicellular roll pattern of stream lines with slightly larger magnitude as compared to the case of $\Omega = 10\ rpm$. The isotherm demonstrates thin boundary layer near isothermal walls with stable stratification of the core as seen in Fig. 8. For $Ra = 1.1 \times 10^5$, radical change in the streamline rolls pattern formation are observed and the streamlines move towards the isothermal wall as shown in Fig. 9. These rolls are primarily formed by the action of coriolis forces on the fluid which offsets the streamline from centre of enclosure, as the coriolis force are much larger than thermal buoyancy. Isotherms in Fig. 9 show generation of spiral shaped structure in the core of the enclosure which leads to strong stable stratification of the core. coriolis forces are more dominant force from centre of hot wall towards the cold wall which leads to the formation of spiral shaped isotherms and significant changes in flow structure are observed with increase in Ra and rotation.

6.2 Effect of Rayleigh Number with Rotation on Flow and Temperature Field in Time Domain

Figure 10 and 11 shows the effect of Rayleigh number with rotation on the flow structure in the time domain in the rotating enclosure. The time histories of temperature and velocity are plotted at a spatial point$(0.25, 0.25)$.

For $\Omega = 10\ rpm$ at $Ra = 1.3 \times 10^4$, initially the instantaneous temperature and velocity are sensitive to time and varies periodically with time. As time progresses, this behaviour disappears and flow becomes steady as depicted in Fig. 10. The similar

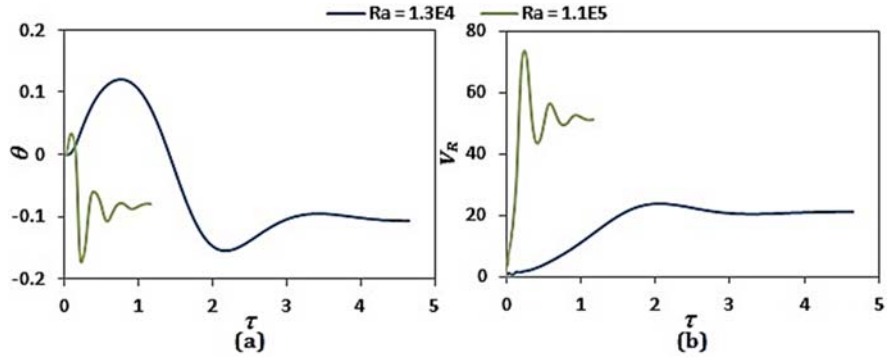

Fig. 10. Time histories of dimensionless temperature with dimensionless time at spatial point $(0.25, 0.25)$ at $\Omega = 10\ rpm$.

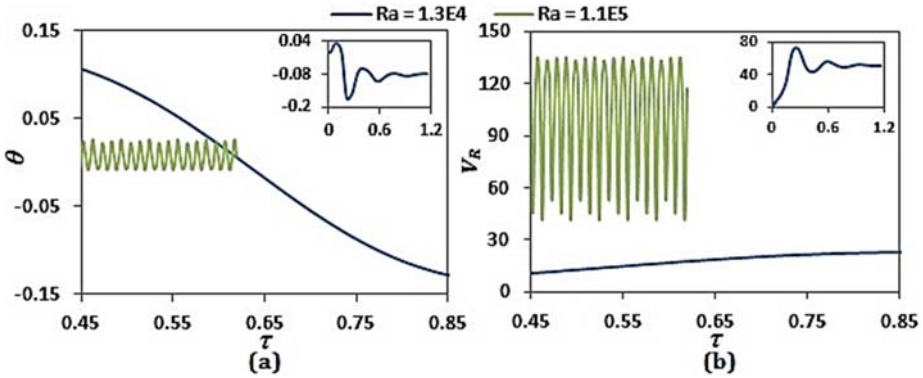

Fig. 11. Time histories of dimensionless temperature with dimensionless time at spatial point $(0.25, 0.25)$ at $\Omega = 25\ rpm$.

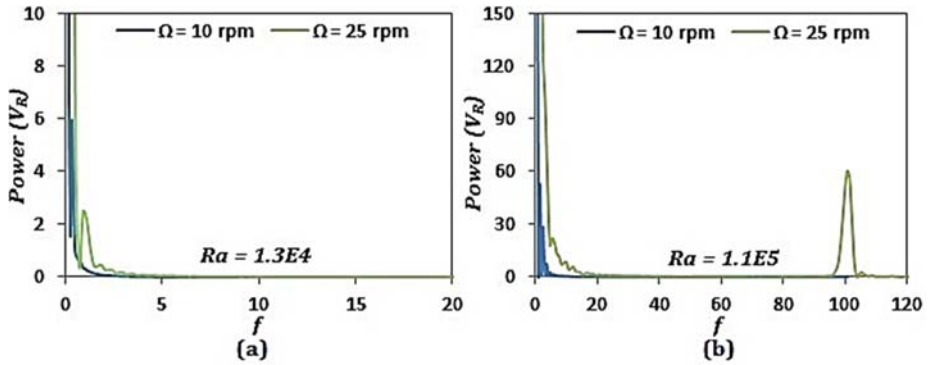

Fig. 12. Power spectral density curves for time series of dimensionless velocity at spatial point (0.25, 0.25) at $\Omega = 10\ rpm$.

trend is observed with further increase in Ra to 1.1×10^5 as shown in Fig. 10. Fig. 10 shows that with increase in Ra, the flow take much longer time to reach steady state.

For $\Omega = 25\ rpm$ at $Ra = 1.3 \times 10^4$, the same trend is observed as that for $\Omega = 10\ rpm$ as shown in Fig. 11a. For $Ra = 1.1 \times 10^5$, the flow becomes periodic in time with large amplitude of oscillation as observed in Fig. 11b. The transients have been removed from these histories and only the long term temporal behaviour found to exist in time has been plotted. The increase in Ra with rotation affects the flow significantly and changes the flow structure from steady state to the time periodic state.

6.3 Effect of Rayleigh Number with Rotation on Frequency Content of Flow Oscillation

To examine the frequency content of these time series, the PSD (Power Spectral Density) are generated as shown in Fig. 12. Each time history has been recorded for a sufficient long time with 2^9 sample points. A FFT is applied to the discrete time history after removing the mean part from the discrete series. The power is then computed as the square of the FFT amplitudes.

For $\Omega = 10\ rpm$ and $Ra = 1.3 \times 10^4$ from the PSD data, it is observed that $f_1 = 1.15$, no

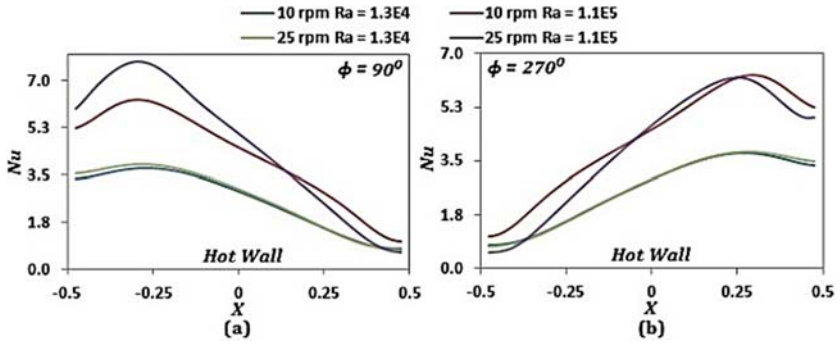

Fig. 13. Variation of Local Nusselt number at Hot wall with dimensionless coordinate for $\Omega = 10\ rpm$.

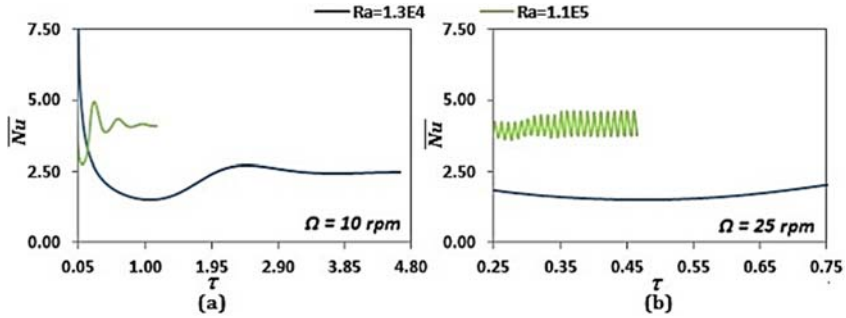

Fig. 14. Variation of space average Nusselt number at hot wall with dimensionless time for $\Omega = 10\ rpm$.

harmonics of f_1 are found in the spectrum as shown in Fig. 12a. This frequency is the fundamental frequency. As no harmonics of f_1 are found in the spectrum as shown in Fig. 12a, the flow becomes steady after initial transient. For $Ra = 1.1 \times 10^5$, it is observed that $f_1 = 1.21$, $f_2 = 2.42$, and $f_3 = 3.63$. f_1 represents the fundamental frequency while f_2 and f_3 are the second and third harmonics. No other peaks of higher harmonics of f_1 are observed in the spectrum as shown in Fig. 12b. The flow becomes steady state after few initial oscillations. Fig. 12 shows that with increase in Ra, the flow take much longer time to reach steady state.

For $\Omega = 25\ rpm$ and $Ra = 1.3 \times 10^4$, from the PSD data, it is observed that $f_1 = 2.69$, no other significant peaks of higher harmonics of f_1 are found in the spectrum as shown in Fig. 12a, thus the flow reaches steady state after initial transient. For $Ra = 1.1 \times 10^5$ from the PSD data, it is observed that $f_1 = 3.02$, $f_2 = 6.05$ and $f_3 = 9.08$. Here also f_1 represents the fundamental frequency while f_2 and f_3 are the second and third harmonics. A peak with significant power at $f_4 = 99.17$ is observed as shown in Fig. 12b. This frequency is not harmonic of f_1 and the flow is characterised by two main unrelated frequencies, suggesting a quasi periodic state. Fig. 12 shows that with increase in Ra and Ω the flow structure changes from steady state to a quasi periodic state.

6.4 Effect of Rayleigh Number with Rotation on Heat Transfer

Figure 13 presents the effect of Rayleigh number (Ra) on local heat transfer (Nu) with rotation for $\phi = 90^o$ and 270^o angular position of the enclosure. For $\Omega = 10\ rpm$ the local heat transfer reaches a maximum at $X = -0.2633$ for $= 1.3 \times 10^4$ ($Nu_{max} = 3.759$), at $X = -0.2951$ for $Ra = 1.1 \times 10^5$ ($Nu_{max} = 6.313$) for $\phi = 90^o$ and at $X = 0.2633$ for $Ra = 1.3 \times 10^4$ ($Nu_{max} = 3.77$), at $X = 0.2951$ for $Ra = 1.1 \times 10^5$ ($Nu_{max} = 6.312$) for $\phi = 270^o$ angular position. For $\Omega = 25\ RPM$ the local heat transfer reaches a maximum at $X = -0.2633$ for $Ra = 1.3 \times 10^4$ ($Nu_{max} = 3.88$), at $X = -0.2951$ for $Ra = 1.1 \times 10^5$ ($Nu_{max} = 7.72$) for $\phi = 90^o$ and at $X = 0.2787$ for $= 1.3 \times 10^4$ ($Nu_{max} = 3.88$), at $X = 0.2951$ for $Ra = 1.1 \times 10^5$ ($Nu_{max} = 6.250$) for $\phi = 270^o$ angular position and then decreases to a minimum as shown in the Fig. 13. The Nu presents similar trend for both Ra with rotation but significant increases in Nu_{max} is observed with increase in Ra and a marginal offset in the peak of Nu_{max} is observed as shown in Fig. 13. The peak value of Nu represents maxima for $Ra = 1.1 \times 10^5$ and minima for $Ra = 1.3 \times 10^4$.

6.5 Effects of Rayleigh Number with Rotation on Space and Time Average Heat Transfer

Figure 14 shows the effect of Rayleigh number (Ra) on space average heat transfer ($\overline{Nu}$) with rotation for $\phi = 90^o$ and 270^o angular position of the enclosure. The transients have been removed from these histories and only the long term temporal behaviour found to exist in time has been plotted. At

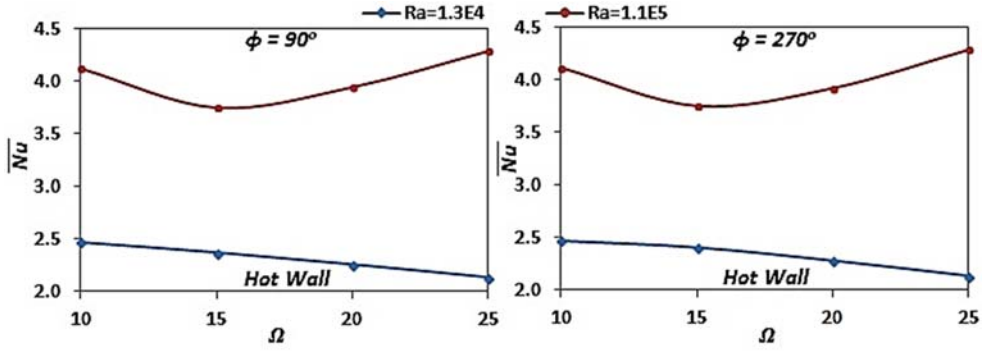

Fig. 15. Variation of space average Nusselt number with rotation.

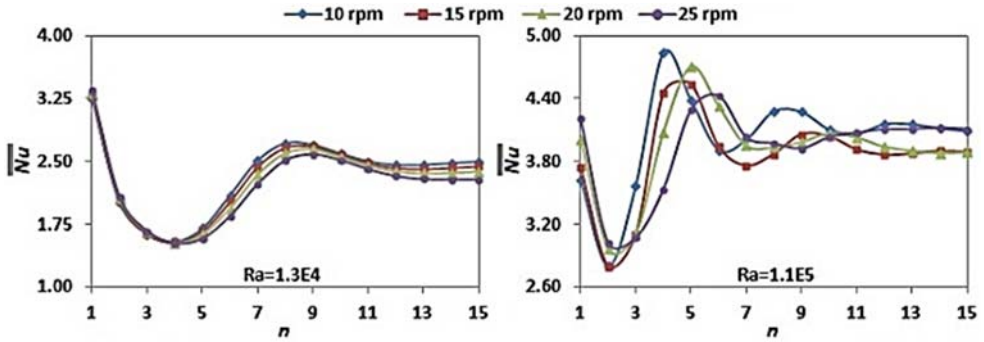

Fig. 16. Variation of time average Nusselt number with number of rotation of the enclosure.

$\Omega = 10\,rpm$, for $Ra = 1.3 \times 10^4$and 1.1×10^5 , Fig. 14 shows that the $\overline{Nu}$ is initially sensitive to time and varies periodically with time. With progress in time, this behaviour disappears and the heat transfer attains steady state and the heat transfer occurs primarily due to diffusion of energy in the enclosure dominated by thermal buoyancy. At $\Omega = 25\,rpm$, for $Ra = 1.3 \times 10^4$, the same trend is continued as shown in Fig. 19. For $Ra = 1.1 \times 10^5$ after initial transients, the $\overline{Nu}$ exhibits cyclic flow pattern with the rotation of the gravity vector as depicted in Fig. 19. The heat transfer now occurs due to the convective motion through the core of the enclosure driven by coriolis force. The periodic variations in $\overline{Nu}$ with time are essentially caused by the harmonic nature of the thermal buoyancy in the flow driven by coriolis force with increased rotational frequency of the gravity vector.

Figure 15 shows the effect of Rayleigh number (Ra) on space average Nusselt number $(\overline{Nu})$ with rotation for $\phi = 90^o$and $\phi = 270^o$ angular position of the enclosure. For $Ra = 1.3 \times 10^4$ at $\Omega = 15\,rpm$, the $\overline{Nu}$ decreases by 4.59% for $\phi = 90^o$ and 4.95% for $\phi = 270^o$ as compared to case of $\Omega = 10\,rpm$. At $\Omega = 20\,rpm$, the $\overline{Nu}$ decreases by 5.58% for $\phi = 90^o$ and 5.78% for $\phi = 270^o$ as compared to $\Omega = 15\,rpm$. At $\Omega = 25\,rpm$, the $\overline{Nu}$ further decreases by 6.83% for $\phi = 90^o$ and 6.58% for $\phi = 270^o$ as compared to $\Omega = 20\,rpm$. Fig. 15 show that the $\overline{Nu}$ decrease with increase in the rotation. The decrease in $\overline{Nu}$ is essentially caused by the opposing interaction of the coriolis force which grows in magnitude with rotation and tends to induce clockwise flow circulations in the thermal buoyancy dominated flow. For $Ra = 1.1 \times 10^5$ at $\Omega = 15\,rpm$, the $\overline{Nu}$ decreases by 9.31% for $\phi = 90^o$ and 9.22% for $\phi = 270^o$ as compared to case of $\Omega = 10\,rpm$. At $\Omega = 20\,rpm$, the $\overline{Nu}$ now increases by 6.42% for $\phi = 90^o$ and 6.35% for $\phi = 270^o$ as compared to $\Omega = 15\,rpm$. At $\Omega = 25\,rpm$, the $\overline{Nu}$ further increases by 10.56% for $\phi = 90^o$ and 11.73% for $\phi = 270^o$ as compared to $\Omega = 20\,rpm$. Fig. 15 show that the $\overline{Nu}$ initially decrease with increase in rotation up to $\Omega = 15\,rpm$, beyond which it increases with increase in the rotation. The $\overline{Nu}$ first decreases to a minimum and then starts to increase with rotation. The minimum varies with the Rayleigh number and corresponds to the balance of the interacting forces at the point of transition from counter clockwise motion to the clockwise motion. At rotation below that for the minimum in the $\overline{Nu}$, the circulation is counter clockwise. The direction of coriolis force is from the core region, so that both flow and heat transfer is reduced. When the coriolis force is much larger than the thermal buoyancy, the motion is clockwise, and the transition is prevented. The coriolis force now promote the flow circulation and therefore increases the $\overline{Nu}$.

For $Ra = 1.3 \times 10^4$and 1.1×10^5, the $\overline{\overline{Nu}}$ initially is sensitive to time and varies periodically with it. As time progresses, this behaviour disappear and the $\overline{\overline{Nu}}$ attains steady state as depicted in Fig. 16. Fig. 16 shows that the flow takes much longer time to reach steady state with increase in Ra. Fig. 16 shows that after about 12 revolutions, the $\overline{\overline{Nu}}$ reaches steady state with time for all Ra and rotations considered in this study.

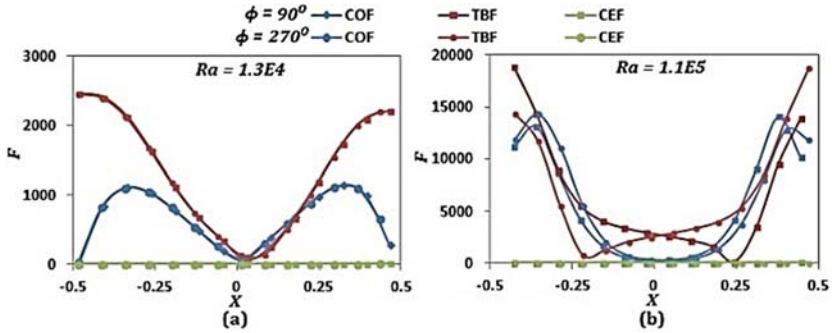

Fig. 17. Variation of coriolis, thermal buoyancy and centrifugal forces with X along mid plane of enclosure for ϕ = 90° at $\Omega = 10\ rpm$.

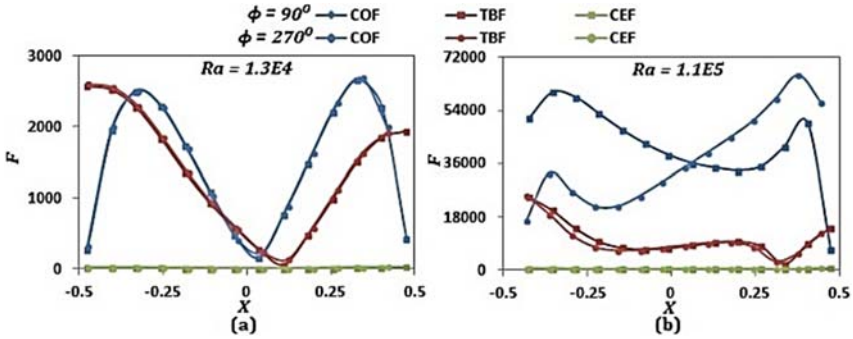

Fig. 18. Variation of coriolis, thermal buoyancy and centrifugal forces with X along mid plane of enclosure for ϕ = 270° at $\Omega = 25\ rpm$.

6.6 Effects of Rayleigh Number with Rotation on Coriolis Force and Thermal Buoyancy

For $\Omega = 10\ rpm$ at $Ra = 1.3 \times 10^4$ Fig. 17 suggests, the flow is close to those driven by thermal buoyancy alone as its magnitude is much larger than coriolis force. The flow circulations are counter clockwise driven by thermal buoyancy. With increase in Ra to 1.1×10^5, the magnitude of coriolis force and thermal buoyancy increases to much greater extent as shown in Fig. 17 Though there is significant increase in these forces with increase in Ra, still the magnitude of coriolis force in much smaller than thermal buoyancy and the flow is still driven by thermal buoyancy. In the thermal buoyancy flow, with increase in the Ra, the flow and heat transfer increase significantly.

For $\Omega = 25\ rpm$ at $Ra = 1.3 \times 10^4$, Fig. 18 show that the magnitude of coriolis force becomes quite comparable with thermal buoyancy. The opposing interaction of counter clockwise and clockwise circulations caused by these forces decreases the heat transfer as shown in Fig. 15. With increase in Ra to 1.1×10^5, the coriolis force are much larger than the thermal buoyancy as depicted in Fig. 18. The flow circulations are clockwise and the transition to counter clockwise is prevented. The coriolis force now promotes the flow circulations and thus increases the heat transfer. Fig. 18 shows that the flow structure changes from the flows solely dominated by thermal buoyancy to the flows completely dominated coriolis force with increase in Ra and rotation.

7. CONCLUSIONS

The detailed study of flow structure and heat transfer characteristics at varying Rayleigh number and rotation reveals different regimes of flow in which different body forces dominate. The range of rotation considered is wide enough to capture a variety of physical behaviour ranging from the dynamics of flow driven solely by thermal buoyancy to the dynamics at rotations, so that the effects of thermal buoyancy becomes insignificant in comparison to coriolis effects. Based on the present investigation, the following conclusions are drawn.

- At $Ra = 1.3 \times 10^4$, for all rotation undertaken in the study, the flow is driven by thermal buoyancy. The $\overline{Nu}$ decreases with increase in rotation and flow becomes steady state after initial transients
- For $Ra = 1.1 \times 10^5$ at $\Omega = 10\ rpm$, The flow is driven by thermal buoyancy and the flow reaches steady state after initial transients. At $\Omega = 15\ rpm$, the flow is driven by both thermal and coriolis force. The opposing interaction of these forces decreases the heat transfer to minimum and the flow becomes periodic in time. At $\Omega = 20\ rpm\ and\ 25\ rpm$, the flow is driven by coriolis force with increase in heat transfer through the core of the enclosure.

The flow becomes quasi periodic in time.

- For $Ra = 1.1 \times 10^5$ at $\Omega = 10\,rpm$ and $15\,rpm$, the $\overline{Nu}$ reaches steady state after initial transients and for $\Omega = 20\,rpm$ and $25\,rpm$, $\overline{Nu}$ become periodic in time.
- With increase in Rayleigh number and rotation, the $\overline{\overline{Nu}}$ takes much longer time to attain steady state. Also after about 12 revolutions, the $\overline{\overline{Nu}}$ reaches steady state.
- For the cases undertaken in this study, the $\overline{Nu}$ attains steady state in thermal buoyancy driven flows. In coriolis force driven flows, the $\overline{Nu}$ varies periodically with time and the flow exhibits cyclic changes with the rotation of gravity vector.
- For all the cases undertaken in this study, the contribution of the centrifugal force is negligible as compared to coriolis force and thermal buoyancy force.
- The FFT or frequency content of time series reveals different classes of flow regime from steady to quasi periodic state with increase in Rayleigh number and rotation. In the flow controlled by thermal buoyancy, the flow becomes steady. In the flow controlled by both thermal buoyancy and coriolis force, the flow becomes periodic in time. In the flow controlled by coriolis force, the flow becomes quasi periodic in time.

REFERENCES

Abell, S. and J. L. Hudson (1975). An experimental study of centrifugally driven free convection in a rectangular cavity, Int. Journal of Heat Mass Transfer 18, 1415–1423.

Baig, M. F. and A. Masood (2001). Natural convection in a two-dimensional differentially heated square enclosure undergoing rotation, Numerical Heat Transfer Part A 40, 181–202.

Baig, M. F. and M. Zunaid (2006). Numerical simulation of liquid metals in differentially heated enclosure undergoing orthogonal rotation, International Journal of Heat and Mass Transfer 49, 3500–3513.

Brooks, I. H. and S. Ostrach (1970). An experimental investigation of natural convection in a horizontal cylinder, Journal of Fluid Mechanics 44, 545–561.

Buhler, K. and H. Oertel (1982). Thermal cellular convection in rotating rectangular boxes, J. Fluid Mech. 114, 261–282.

Hamady, F. J., J. R. Lloyd, K. T. Yang and H. Q. Yang, (1994). A study of natural convection in a rotating enclosure, J. Heat Transfer 116, 136–143.

Homsy, G. M. and J. L. Hudson. (1971). Heat transfer in a rotating cylinder of the fluid heated from above, Int. Journal of Heat Mass Transfer 14, 1049–1159.

Jin, L. F., S. K. W. Tou and C. P. Tso (2005). Effects of rotation on natural convection cooling from three rows of heat sources in a rectangular cavity, International Journal of Heat and Mass Transfer 48, 3982–3994.

Ker, Y. T. and T. F. Lin (1996). A combined numerical and experimental study of air convection in a differentially heated rotating cubic cavity, International Journal of Heat and Mass Transfer 39, 3193–3210.

Ker, Y. T. and T. F. Lin (1997). Time-averaged and reverse transition in oscillatory air convection in a differentially heated rotating cubic cavity, International Journal of Heat and Mass Transfer 40, 3335–3349

Kuppers, G. and D. lortz (1969). Transition from laminar convection to thermal turbulence in a rotating fluid layer, Journal of Fluid Mechanics 35, 609–620.

Lee, T. L. and T. F. Lin (1996). Transient three-dimensional convection of air in a differentially heated rotating cubic cavity, International Journal of Heat and Mass Transfer 39, 1243–1255.

Mandal, J. C. and C. R. Sonawane (2013). Simulation of flow inside differentially heated rotating cavity, International Journal of Numerical Methods for Heat and Fluid Flow 23(1), 23-54.

Mori, Y., T. Fukada and W. Nakayama (1971). Convective heat transfer in a rotating radial circular pipe, Int. Journal of Heat Mass Transfer 14, 1027–1040.

Nadeem, H. and S. Sangh (2004). The dynamics of two dimensional buoyancy driven convection in a horizontal rotating cylinder, Journal of Heat Transfer 126, 963–984.

Nadeem, H. and S. Sanghi (2007). On the role of Coriolis force in a two dimensional thermally driven in a rotating enclosure, Journal of Heat Transfer 129, 179–187.

Narendra Kumar, M., G. Pundarika, K. Rama Narasimha and K. N. Seetharamu (2016). Effect of Rotation on Natural Convection in Differentially Heated Rotating Enclosure by Numerical Simulation, Journal of Applied Fluid Mechanics 9(3), 1265–1272.

Ostrach, S. (1950). A boundary layer problem in the theory of free convection, Doctoral Thesis, Brown University.

Pfotenhauer, J. M., J. J. Niemela and R. J. Donnelly (1987). Stability and heat transfer of rotating cryogens. Part 3. Effects of finite cylindrical geometry and rotation on the onset of convection, Journal of Fluid Mechanics 175, 85–96.

Rossby, H. T**. (**1969). A study of Benard convection with and without rotation**, J.** Fluid Mech. 36, 309-335.

Tso, C. P., L. F. Jin and S. K. W. Tou (2007). Numerical segregation of the effects of body forces in a rotating, differentially heated enclosure ,Numerical Heat Transfer Part A 51, 85–107.

Vanyo, J. P. (1993). Rotating Fluids in Engineering and Science, Butterworth-Heinemann Press.

Veronis, G. (1968). Large amplitude benard convection in a rotating fluid", Journal of Fluid Mechanics 31, 113–139.

Weinbaum, S. (1964). Natural convection in a horizontal cylinder, Journal of Fluid Mechanics 18, 409–437.

Xin, S., P. Le Quere and O. Daube (1997). Natural convection in a differentially heated horizontal cylinder: effects of Prandtl number on flow structure and instability, Physics Fluid 4, 1014–1033.

Y. Masuda , A. Suzuki, Y. Mikawa, Y. Kagamitani, T. Ishiguro, C. Yokoyama and T. Tsukada (2010). Numerical simulation of GaN single-crystal growth process in ammono-thermal autoclave – Effects of baffle shape" International Journal of Heat and Mass Transfer 53, 940–943.

Yin, C. P., Y. T. Ker, T. H. Huang and T. F. Lin (2001), Fluctuating characteristics and rotation induced stabilization of thermal buoyancy driven water flow in a vertical rotating cylinder, International Journal of Heat and Mass Transfer 44, 919–930.

Yoshio Masuda, A., O. Sato, D. Tomida and C. Yokoyama (2016), Convection patterns and temperature fields of ammonothermal GaN bulk crystal growth process, Japanese Journal of Applied Physics 55, 05FC03.